Chem

Article

Electrified CO_2 uptake in quinone-based covalent organic frameworks

Graphical abstract

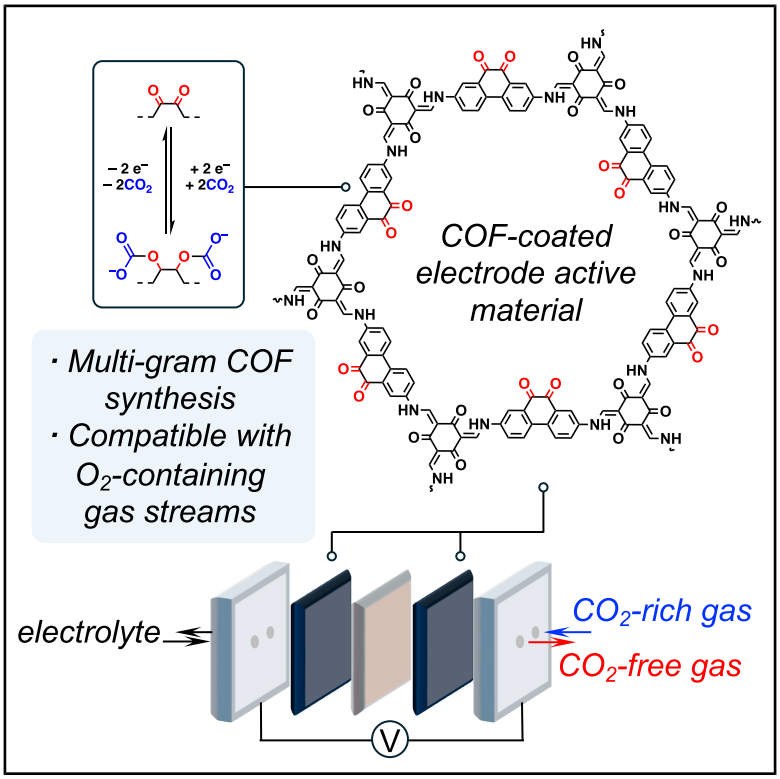

Highlights

- Gram-scale open-flask synthesis of crystalline quinone-based COFs
- COFs shift quinone redox potentials away from the oxygen-reduction region
- Stable CO_2 capture in an MEA device for 80 h under simulated flue gas
- Energy-efficient operation achieving 7.5 GJ per ton of CO_2.

Authors

Mohammad K. Shehab, Chuanhui Huang, Zeyan Liu, ..., Ke Xie, Edward H. Sargent, Omar K. Farha

Correspondence

kent.kirlikovali@northwestern.edu (K.O.K.), ke-xie@northwestern.edu (K.X.), ted.sargent@northwestern.edu (E.H.S.), o-farha@northwestern.edu (O.K.F.)

In brief

Electrochemical CO_2 capture using molecular quinones is often limited by solubility and oxygen sensitivity in liquid systems. Embedding quinones into porous covalent organic frameworks (COFs) enhances stability, shifts reactivity into an oxygen-tolerant regime, and localizes redox activity to the solid sorbent. We developed a scalable synthesis of quinone-based COFs and validated their performance in a device operating under simulated flue gas, capturing CO_2 efficiently for 80 h. This approach offers a promising, solid-state pathway toward electrochemical carbon-capture technologies.

Shehab et al., 2026, Chem *12*, 102910
June 11, 2026
https://doi.org/10.1016/j.chempr.2025.102910

CellPress

Please cite this article in press as: Shehab et al., Electrified CO_2 uptake in quinone-based covalent organic frameworks, Chem (2025), https://doi.org/10.1016/j.chempr.2025.102910

Chem

CellPress

Article

Electrified CO_2 uptake in quinone-based covalent organic frameworks

Mohammad K. Shehab,[1,2,6] Chuanhui Huang,[2,6] Zeyan Liu,[2] Xijun Wang,[1] Yuyin Li,[2] Kent O. Kirlikovali,[1,2,*] Ke Xie,[1,2,3,*] Edward H. Sargent,[1,2,3,4,*] and Omar K. Farha[1,2,4,5,7,*]

[1]International Institute for Nanotechnology, Northwestern University, Evanston, IL 60208, USA
[2]Department of Chemistry, Northwestern University, Evanston, IL 60208, USA
[3]Department of Electrical and Computer Engineering, Northwestern University, Evanston, IL 60208, USA
[4]Paula M. Trienens Institute for Sustainability and Energy, Northwestern University, Evanston, IL 60208, USA
[5]Department of Chemical & Biological Engineering, Northwestern University, Evanston, IL 60208, USA
[6]These authors contributed equally
[7]Lead contact
*Correspondence: kent.kirlikovali@northwestern.edu (K.O.K.), ke-xie@northwestern.edu (K.X.), ted.sargent@northwestern.edu (E.H.S.), o-farha@northwestern.edu (O.K.F.)
https://doi.org/10.1016/j.chempr.2025.102910

THE BIGGER PICTURE Capturing carbon dioxide efficiently and at low cost remains one of the biggest challenges in mitigating climate change. Many existing carbon-capture technologies rely on heating large volumes of chemicals to release CO_2, which consumes significant energy and leads to degradation of the sorbent materials over time. Electrified carbon capture offers a promising alternative by using electricity, rather than heat, to drive reversible CO_2 binding. However, current electrochemical systems often depend on small molecules that dissolve into the electrolyte, becoming unstable and requiring large electrical inputs to activate.

Our work addresses these limitations by directly incorporating CO_2-binding units, quinones, into a solid, porous material called a covalent organic framework (COF). Unlike molecular quinones, the COF-based systems do not dissolve, can be synthesized in gram-scale batches using our newly reported, straightforward open-flask method, and display enhanced electronic properties that make CO_2 capture more energy-efficient. The extended framework also shifts the quinone redox potentials to a regime that avoids unwanted oxygen-reduction reactions, an essential requirement for operation under realistic flue-gas conditions.

We integrated our most promising COF, DADOP-TFP, into a membrane electrode assembly and demonstrated stable CO_2 capture and release for 80 h under simulated industrial gas streams in the presence of O_2. Importantly, the system achieves an energy consumption of only 7.5 GJ per ton of CO_2, competitive with or lower than many emerging electrochemical approaches. By pairing scalable synthesis with device-level validation, this work suggests a viable route toward electrified carbon-capture modules that are modular, durable, and suitable for distributed deployment. More broadly, the strategy of embedding redox-active molecules into crystalline porous frameworks for electrified CO_2 capture opens new opportunities for designing solid-state sorbents for clean-energy applications.

SUMMARY

Rising atmospheric CO_2 levels demand energy-efficient, durable capture technologies. Quinones are promising redox-active materials that can reversibly bind CO_2. However, molecular quinones require functionalization to avoid side reactions with oxygen, and electroreducing them in liquid-phase systems requires applying a potential across the bulk solution, consuming excess charge and energy. We envisioned that incorporating quinones into solid-state sorbents would shift the redox potential via electron delocalization and decrease the needed charge by localizing electroreduction within the active material. Here, we report a scalable, open-flask synthesis of highly porous, crystalline quinone-based covalent organic frameworks (COFs) that yield grams per batch. Integrated into a membrane electrode assembly (MEA), the COF, DADOP-TFP, operates for 80 h under simulated flue-gas conditions with an energy cost of 7.5 GJ/ton CO_2.

Please cite this article in press as: Shehab et al., Electrified CO_2 uptake in quinone-based covalent organic frameworks, Chem (2025), https://doi.org/10.1016/j.chempr.2025.102910

INTRODUCTION

The increasing levels of CO_2 in the atmosphere, primarily driven by human activities such as burning fossil fuels and deforestation, have intensified the greenhouse effect, leading to climate change.[1,2] It disrupts ecosystems, contributes to ocean acidification, and poses risks to biodiversity, agriculture, and human health. In carbon capture and storage (CCS), CO_2 is extracted from industrial point sources before it enters the atmosphere for underground storage or repurposing.[3–7] Sorbent materials have been developed for CO_2 capture based on chemisorption and physisorption.[8–11] Chemisorption, which involves chemical bond formation between CO_2 and the sorbent, results in stronger and more selective interactions with CO_2 compared to physisorption, which occurs through non-covalent interactions between CO_2 and the surface of the sorbent. A widely studied chemisorption-based CO_2 capture is the wet chemical scrubbing process, which utilizes aqueous amines to absorb CO_2 in a 2:1 ratio (NH_2:CO_2) and then releases it through a temperature-swing process. It is effective at capturing CO_2 but suffers from sorbent degradation and corrosion due to the high pH of the amine solution. Porous materials with nanometer-sized pores, such as metal-organic frameworks (MOFs), activated carbon, and zeolites, typically rely on physisorption, and thus offer lower heats of adsorption; however, their selectivity and CO_2 capture efficiency are limited in low-CO_2-concentration environments.[8]

Electrochemically driven carbon capture has gained attention for its ability to operate at lower temperatures and ambient pressure. Several electrochemical methods have been explored, including supercapacitive swing adsorption (SSA),[12–14] pH swing techniques,[15,16] and redox-active molecules that bind CO_2 when electrochemically reduced.[17–22] Quinones are widely used as redox-active molecules for electrochemical CO_2 capture due to their highly reversible redox processes, which enable selective capture of CO_2 in their reduced form and subsequent release of CO_2 upon oxidation to their neutral form (Figure 1A).[18] The quinone capture/release mechanism relies on electrochemically sweeping the potential rather than applying heat, potentially facilitating decentralized deployment via modular system design. Quinones have demonstrated effectiveness across different systems, including solutions, solid electrodes, and flow cells.[17–19,22,23]

A challenge for molecular quinones used in solid-state CO_2 capture devices is their high solubility in organic electrolytes, which reduces their efficacy following repeated capture/release cycling.[24] For example, Wielend et al. demonstrated that while thin-film quinone electrodes captured CO_2 efficiently during the initial cycles, prolonged cycling led to significant quinone leakage into the electrolyte.[24] Beyond durability concerns, liquid-phase systems also suffer from inefficiencies that arise from applying an electrical potential across the entire electrolyte volume as needed to electroreduce dissolved quinones, thereby increasing the energy cost per mole of CO_2 captured. This bulk-phase reduction approach lacks the spatial selectivity of solid-state systems, wherein charge can be localized at redox-active sites.

Researchers have sought to address these limitations by synthesizing quinone-based polymers as solid-state CO_2 capture materials and integrating them into a composite electrode with carbon nanotubes, which increased the stability of devices to 7,000 cycles.[19] Hartley et al. developed quinone-functionalized porous carbon materials for electrochemically driven CO_2 capture to overcome solubility issues.[18] Monomeric quinones require reduction potentials more negative than that for the reduction of O_2 to superoxide (O_2^-), making this reaction a competing side process in the presence of ambient or dissolved oxygen. While O_2 is not directly involved in the CO_2 capture mechanism, the superoxide is reactive and can degrade the sorbent. For this reason, researchers anodically shift the quinone redox potentials away from the O_2 reduction region by functionalizing the quinone core with electron-withdrawing groups.[22] Although these modifications have proven effective toward this goal, functionalized quinones often still face solubility issues in organic electrolytes, posing challenges for their use in solid-state devices.[22]

We hypothesized that integrating quinone molecules into extended framework structures would address the solubility concern while simultaneously shifting the reduction potential to more positive values, i.e., away from the O_2 reduction regime, the result of extended conjugation and enhanced electron delocalization. Specifically, we envisioned synthesizing quinone-based covalent organic frameworks (COFs), which are permanently porous two- or three-dimensional organic materials composed of repeating units connected by strong covalent bonds.[25] Their robust cross-linked networks would inhibit dissolution in electrolyte solutions, while their porosity, highly ordered crystalline structures,[26] and π-conjugated backbones[27] would enhance CO_2 accessibility to the quinone-based active sites.[28,29] Our computational studies revealed that the quinone-based COF exhibits a significantly narrower highest occupied crystal orbital (HOCO)-lowest unoccupied crystal orbital (LUCO) gap (0.1 eV) compared to the monomeric quinone (0.6 eV), indicating enhanced electronic delocalization within the extended π-conjugated framework (Figure 1B). Importantly, this delocalization is expected to facilitate charge transport and stabilize the reduced state, thereby shifting the reduction potential to more positive values outside the O_2 reduction region. In addition to their tunable electronic properties, COFs offer structural diversity, chemical stability, and well-defined porosity, enabling their application in various fields over the past decade, including gas separation,[30,31] catalysis,[32] heavy metal removal,[33–35] drug delivery,[36] proton conduction,[37] pseudocapacitors,[26,38] and energy storage.[39–42] These combined structural and electronic features of COFs position them as promising candidates for electrochemically mediated CO_2 capture (EMCC). However, high-quality COF samples with high crystallinity and porosity are typically synthesized using solvothermal methods in sealed tubes, which often yield small batch sizes (<50 mg), posing significant challenges for scalability and practical deployment. Overcoming this synthetic bottleneck is essential to produce sufficient quantities of material to test our hypothesis regarding quinone-based COFs for CO_2 capture in an electrochemical device and to enable their ultimate end-use at scale. Therefore, we first set out to develop a scalable synthesis

Please cite this article in press as: Shehab et al., Electrified CO_2 uptake in quinone-based covalent organic frameworks, Chem (2025), https://doi.org/10.1016/j.chempr.2025.102910

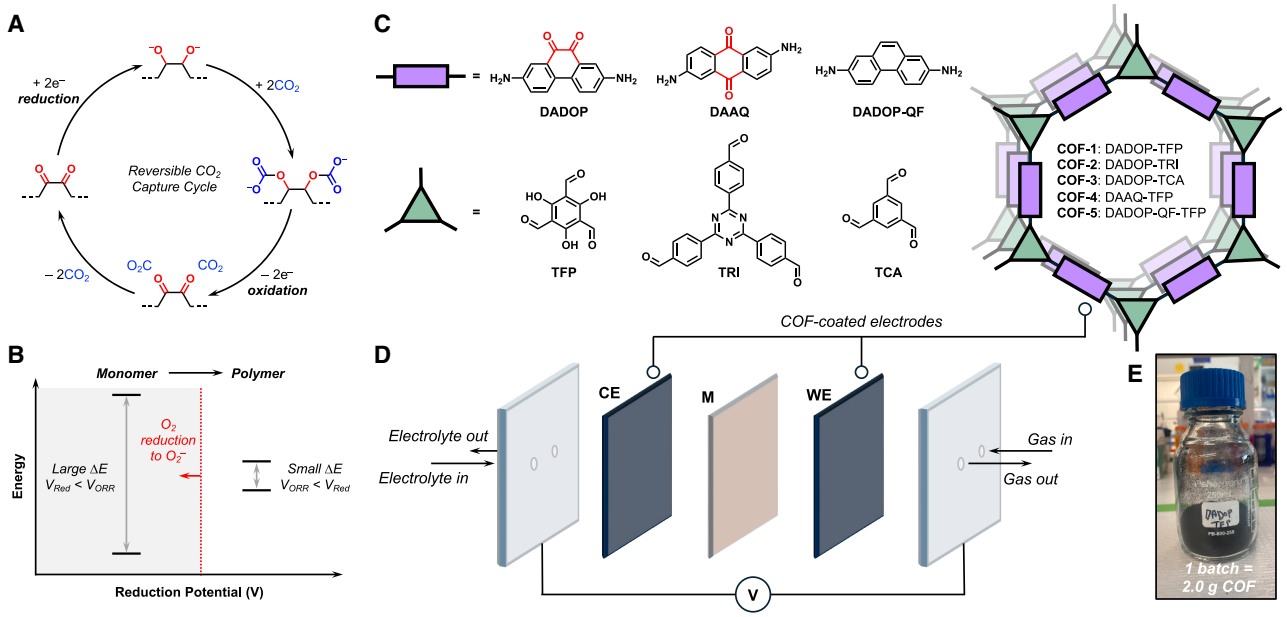

Figure 1. Schematic diagrams

(A) A reversible redox cycle enables quinones to capture and release CO_2 through electrochemical reduction and oxidation reactions.

(B) Energy band diagrams for the quinone monomer and the quinone-based COF.

(C) COFs synthesized using the large-scale solvothermal method in this work.

(D) Membrane electrode assembly device (CE, counter electrode; M, membrane; and WE, working electrode).

(E) Photograph of a multi-gram batch of DADOP-TFP.

route capable of producing gram-scale quantities of crystalline, porous quinone-based COFs.

RESULTS AND DISCUSSION

To begin our investigation, we targeted imine-linked COFs constructed from amine-functionalized quinone building blocks and complementary aldehyde-based linkers (Figure 1C). The formation of imine-linked COFs relies on the reversible condensation of amines and aldehydes, where reversibility is essential for error correction and the growth of highly ordered and crystalline frameworks. Conventionally, this reversibility is maintained under solvothermal conditions in sealed ampules, where the confined headspace preserves volatile components, stabilizes equilibrium, and promotes extended crystallinity. However, this approach severely limits scalability to yields of about 30 mg per batch,[43] as sealed vessels constrain the reaction volume and introduce challenges for achieving uniform heating and reproducibility. Moreover, the reversible bond formation generates water as a byproduct, which must be carefully managed to prevent premature termination or hydrolysis of the framework. We hypothesized that conducting the reaction in an open round-bottom flask, using methyl-2-pyrrolidone (NMP) as the solvent, acetic acid as a modulator, and water intentionally added as a reaction additive, could support reversible bond formation and crystallinity without requiring a sealed vessel. By leveraging a water-rich environment within a controlled solvent system rather than excluding water, we aimed to maintain dynamic reversibility while enabling a more scalable and practical synthesis route. This approach would promote imine exchange and error correction during framework formation, thereby preserving crystallinity, even at large scales.

To overcome these limitations, we developed a synthetic procedure that enables the multi-gram-scale synthesis of COFs while maintaining the same crystallinity and porosity as the ampule method (Figure 1E). Specifically, we developed optimized conditions to synthesize a quinone-based COF, DADOP-TFP, which is composed of 2,7-diaminophenanthrene-9,10-dione (DADOP monomer) and 2,4,6-trihydroxybenzene-1,3,5-tricarbaldehyde (TFP) (Figure 2A). The reaction was prepared in an open 250-mL round-bottom flask using NMP as the solvent, acetic acid as the modulator, and a stoichiometric excess of amine linker. Water was added as an additive to promote reversible imine formation under ambient conditions. The reaction mixture was then subjected to a mild thermal ramp, reaching 140°C over several days. Solvent exchange and subsequent supercritical CO_2 activation provided 2.0 g of highly crystalline, porous COF material (Figure 2).

Following the isolation of DADOP-TFP, powder X-ray diffraction (PXRD) analysis and N_2 sorption measurements were conducted to assess the crystallinity and porosity, respectively (Figure 2). The PXRD pattern exhibits sharp, well-defined peaks consistent with the simulated pattern, confirming long-range order and the periodicity in the *xy* plane. To assess the stacking formation of the 2D layers, we simulated both the AA (eclipsed) and AB (staggered) stacking models. The Pawley refinement of the AA stacking model for the DADOP-TFP COF was carried out, and the refinement parameters, profile R-factor (R_p), and the weighted profile R-factor

Please cite this article in press as: Shehab et al., Electrified CO_2 uptake in quinone-based covalent organic frameworks, Chem (2025), https://doi.org/10.1016/j.chempr.2025.102910

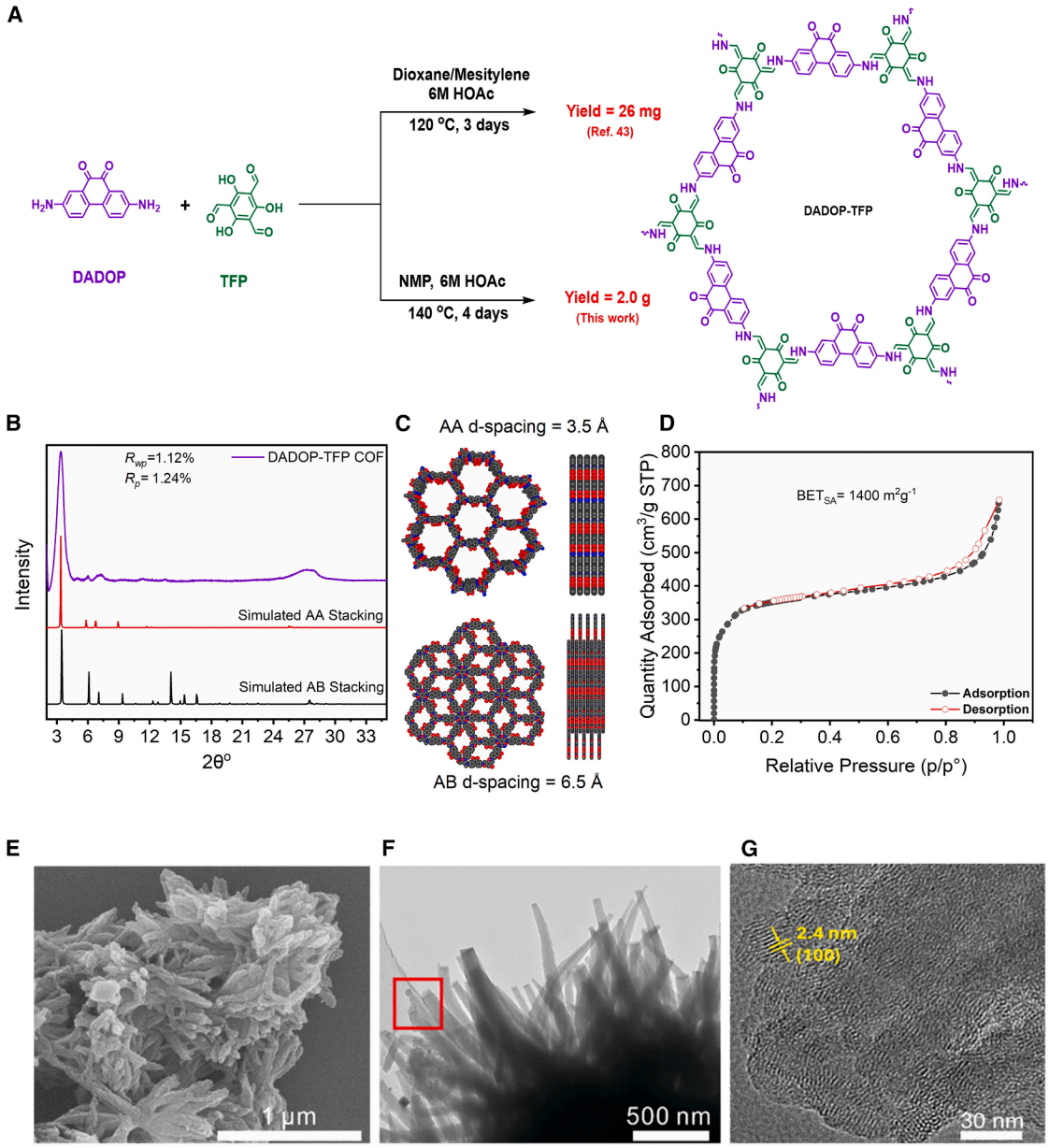

Figure 2. DADOP-TFP characterization

(A) Schematic reaction of DADOP-TFP using an ampule with a yield of 26 mg,[43] and our scaled-up synthesis method using a 3-neck flask with a 2.0 g yield.

(B) PXRD patterns, where the experimental is in purple, the Pawley refinement is in green, the simulated PXRD patterns for the AA eclipsed in red, and AB staggered structures in black.

(C) AA and AB stacking space-filling models showing high quinone decoration of the channels; brown (C), red (O), blue (N), and hydrogens were omitted for clarity.

(D) N_2 adsorption/desorption isotherm with BETSI of 1,342 m^2 g^{-1}.

(E) Scanning electron microscope (SEM) image of the DADOP-TFP (scale bar, 1 μm).

(F) TEM image of the DADOP-TFP (scale bar,500 nm).

(G) High-resolution TEM of lattice fringe image of the 100 planes of DADOP-TFP (scale bar, 30 nm).

(R_{wp}) were calculated. The unit cell lattice parameters were a = b = 30.13 Å, c = 3.48 Å, and angles α = β = 90°, γ = 120°, with a space group of P6/m. The R_p and R_{wp} were 1.24% and 1.12%, respectively (Table S5). In contrast, the AB stacking model employed the $P6_3/mmc$ space group, with lattice parameters a = b = 28.56 Å and c = 6.46 Å and angles α = β = 90°, γ = 120°. The experimental PXRD pattern for DADOP-TFP closely aligns with the simulated pattern of the eclipsed (AA) model, indicating a well-ordered structure along the *z* axis (001) (Figures 2B and 2C). Distinct reflections observed in the experimental PXRD pattern at 3.4°, 5.83°, 6.80°, and 26.0° correspond to the (100), (110), (220), and (001) facets, respectively. Next, N_2 sorption measurements were performed

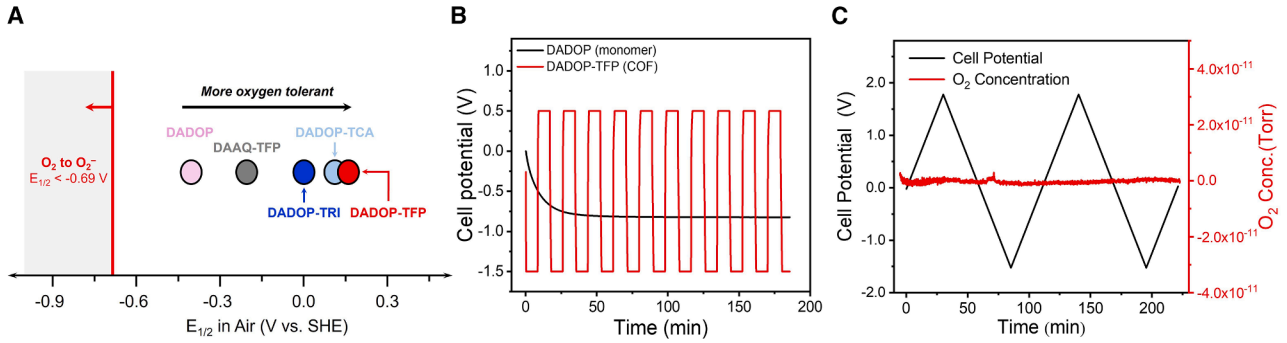

Figure 3. Redox behavior and oxygen tolerance of quinone-based COFs

(A) Half-wave potentials ($E_{1/2}$) obtained from cyclic voltammetry (CV) experiments under air exhibit positive shifts of the COF composite electrodes away from the O_2 reduction region relative to those of the quinone monomers, with DADOP-TFP showing the most positively shifted potential.

(B) Potential sweep profiles for DADOP-TFP and its corresponding DADOP monomer show reversible redox behavior for the COF and irreversible behavior for the monomer.

(C) *In situ* electrochemical mass spectrometry (EC-MS) tracking of O_2 concentration during cyclic voltammetry scanning with DADOP-TFP at a scan rate of 1 mV s^{-1}.

at 77 K to examine the permanent porosity of DADOP-TFP. The Brunauer-Emmett-Teller (BET) surface area was calculated using the BET surface identification (BETSI) computational method to be 1,342 m^2 g^{-1} (Figures 2D and S24–S28).[44] Scanning electron microscopy (SEM) and transmission electron microscopy (TEM) images (Figures 2E and 2F) reveal that DADOP-TFP crystallizes into rod-like particles with lengths of 200–600 nm and diameters of 50–100 nm. High-resolution TEM (HRTEM) further confirmed its crystalline nature, illustrating a lattice fringe with an interplanar spacing of 2.4 nm corresponding to the (100) plane (Figure 2G).

Finally, we tested the generality of this open-flask synthesis method by preparing four additional COFs, including three quinone-based COFs (DADOP-TRI, DADOP-TCA, and DAAQ-TFP, where TRI is 4,4′,4″-(1,3,5-triazine-2,4,6-triyl)tribenzaldehyde, TCA is benzene-1,3,5-tricarbaldehyde, and DAAQ is 2,6-diaminoanthracene-9,10-dione), as well as a quinone-free analog of DADOP-TFP (denoted as DADOP-QF-TFP), which were each synthesized on at least an 800-mg scale (Figure 1C). All materials were obtained under the same reaction conditions in a three-neck flask and exhibited high crystallinity and porosity comparable to those produced by conventional sealed-ampule methods (Figures 2, S13, S15, S17, S19, and S21). With these defined crystalline materials in hand, we next turned to evaluating their electrochemical properties to assess their suitability for CO_2 capture applications.

Electrochemistry of quinone-based COFs

To evaluate the electrochemical behavior of the four quinone-based COFs, we first needed to overcome their intrinsically low electrical conductivity. We addressed this by formulating composite electrodes containing conductive carbon black and Nafion. While direct growth of COFs on carbon nanotubes could, in principle, enhance conductivity, our electrode preparation involves grinding and sonication steps, which would fragment the nanotubes into small carbon pieces and diminish their long-range conductive pathways. Instead, we adopted a composite-ink formulation using carbon black, which is fully compatible with our fabrication process, scalable across multiple COFs, and ensures uniform electrode preparation. This approach ensured efficient electron transport through the extended conjugated frameworks, enabling stable redox reversibility and favorable CO_2 capture/release performance in the membrane electrode assembly (MEA) device. To this end, we prepared composite inks by mixing each COF with carbon black and Nafion in isopropanol. These inks were spray-coated onto carbon paper to fabricate electrodes for testing. Although the studied COFs are inherently hydrophilic, incorporation into the carbon black-Nafion composite rendered the surface hydrophobic. This was confirmed by contact angle measurements, which showed that all COF-based electrodes exhibited contact angles above 90°, indicating poor wetting (Figure S29). This hydrophobicity hinders effective interaction between the redox-active sites and the electrolyte, so we implemented a simple wetting treatment using a methanol-water mixture prior to incorporation into the MEA device (see supplemental information, Section S3 for details). We then collected cyclic voltammograms, which revealed that all four COFs exhibited excellent redox reversibility (Figure S30) and a substantial positive shift in their half-wave potentials ($E_{1/2}$) relative to their monomeric counterparts (Figures 3A and S31). This positive shift is critical since it reduces the overlap with the O_2 reduction region and enhances selectivity for CO_2 capture. In *N*,*N*-dimethylformamide (DMF), O_2 reduction to O_2^- occurs at −1.3 V vs. ferrocenium/ferrocene (Fc^+/Fc),[22] or −0.69 V vs. standard hydrogen electrode (SHE).[45] Therefore, to avoid unwanted O_2^- formation, the cathodic operating potential must be more positive than −0.69 V vs. SHE. A more positive $E_{1/2}$ allows for a deeper reduction of quinone groups without onsetting O_2 reduction, promoting the CO_2 capture coulombic efficiency. Among the COFs studied, DADOP-TFP exhibited the most significant positive shift in $E_{1/2}$, implying the highest tolerance toward oxygen interference (Figure 3A). Specifically, the $E_{1/2}$ increased from −0.469 V for the amine monomer (2,7-diaminophenanthrene-9,10-dione) to +0.095 V for the COF, representing a substantial shift away from the O_2 reduction region. In addition, we compared the redox cycling behavior of DADOP-TFP and its monomer under repeated potential sweeps from −1.5 V

Please cite this article in press as: Shehab et al., Electrified CO_2 uptake in quinone-based covalent organic frameworks, Chem (2025), https://doi.org/10.1016/j.chempr.2025.102910

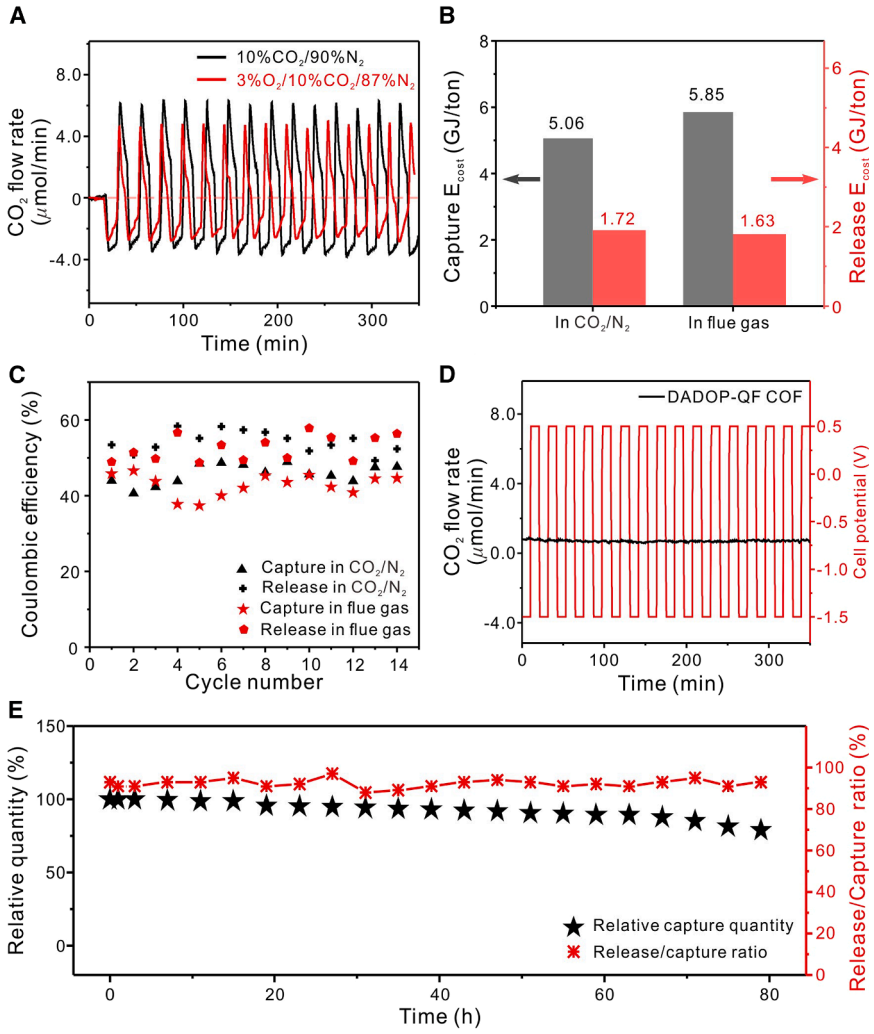

Figure 4. Electrochemical CO_2 capture and release performance of DADOP-TFP in an MEA device

(A) CO_2 readings at the exit of the working electrode over repeated capture and release cycles under N_2 (10% CO_2/90% N_2) and flue gas (3% O_2/10% CO_2/87% N_2) (the CO_2 flow rate readings were normalized to the baseline).

(B) Comparison of energy costs under simulated CO_2/N_2 and flue gas. Left is the average energy cost in the capture process, and right is the average energy cost in the release process.

(C) CO_2 capacity utilization and coulombic efficiency (capture and release) of the system for 14 capture-release cycles.

(D) CO_2 readings at the exit of the working electrode over charging and discharging under flue-gas conditions (3% O_2/10% CO_2/87% N_2) with DADOP-QF-TFP.

(E) Long-term durability over 80 h in flue-gas flow. The device was subjected to a complete capture and release voltage cycle with continuous flue-gas flow. The CO_2 release performance was stable throughout the 80 h of the test.

to 0.5 V (Figure 3B). DADOP-TFP exhibited a stable and reversible electrochemical response over multiple cycles, indicating excellent redox stability, likely due to the structural robustness of the COF. In contrast, the DADOP monomer could not be swept back to positive voltages once driven to negative potential. This poor reversibility suggests irreversible decomposition or side reactions that prevent redox cycling.

Mechanistic investigations of oxygen and quinones

Encouraged by the favorable redox properties, oxygen tolerance, and predicted CO_2 capture properties of DADOP-TFP, we next evaluated its electrochemical CO_2 capture performance in an MEA device. To prepare the COF electrode, the spray-coated DADOP-TFP composite was treated with a methanol-water mixture to improve hydrophilicity and facilitate electrolyte infiltration (Figure S32). The resulting electrode had a thickness of approximately 270 μm and a loading of ~10 mg composite/cm^2 (Figures S33C and S33D). The MEA device was then constructed by using two identical COF-coated electrodes as both the working and counter electrodes (Figures 1D and S34), with 0.5 M Na_2SO_4 buffered with Na_2HPO_4 to a pH of ~7.0, serving as the electrolyte solution. This setup enabled us to assess the intrinsic performance of DADOP-TFP through cyclic CO_2 capture and release operations.

To investigate the mechanism of electrochemical CO_2 capture and to rule out oxygen reduction occurring under these device operating conditions, we employed *in situ* electrochemical mass spectrometry (EC-MS), a real-time technique that enables the direct detection of gaseous species evolved or consumed during electrochemical reactions. While sweeping the potential in cycles from −1.5 V to +1.8 V, we continuously monitored the signal corresponding to molecular oxygen (m/z = 32) in the gas stream. If O_2 reduction occurred, we would expect a measurable decrease in the O_2 signal as molecular oxygen is consumed. As shown in Figure 3C, no significant change in the O_2 signal was detected, indicating that O_2 reduction does not occur under these conditions. This result corroborates our earlier electrochemical results showing a positive half-wave potential ($E_{1/2}$) well separated from the O_2 reduction region and confirms the high oxygen tolerance of DADOP-TFP under the MEA device operating conditions. To further validate this oxygen tolerance, cyclic voltammograms were recorded under both simulated flue gas and pure-nitrogen atmospheres (Figure S35). The nearly identical cyclic voltammograms obtained under both conditions confirm the absence of competing oxygen reduction within the operating potential range (−1.5 V to +1.0 V).

Performance of DADOP-TFP COF in CO_2 capture and release

When the cell potential was swept between −1.5 V and 0.5 V during 8-min cycles, we observed variations in the CO_2

Please cite this article in press as: Shehab et al., Electrified CO_2 uptake in quinone-based covalent organic frameworks, Chem (2025), https://doi.org/10.1016/j.chempr.2025.102910

Table 1. CO_2 capture metrics and energy cost

Gas composition	Coulombic efficiency, capture (%)	Energy cost, capture ($GJ/ton_{capture}$)	Coulombic efficiency (%)	Energy cost, release ($GJ/ton_{release}$)	Energy cost, total (GJ/ton_{total})[a]
10% CO_2 and 90% N_2	46	5.1	55	1.7	6.8
10% CO_2, 87% N_2, and 3% O_2	43	5.9	54	1.6	7.5

[a]Experiments performed in the MEA device using DADOP-TFP using a gas flow rate of 10 sccm, a current of 2 mA cm^{-2}, and a voltage range of −1.5 to 0.5 V.

concentration at the outlet of the working electrode (Figure 4A). During the capture step, electrochemical reduction of the COF generated nucleophilic quinone species (semiquinones or radical anions) that reacted with electrophilic CO_2 to form stable COF-CO_2 adducts.[19,23] This led to a measurable decrease in CO_2 concentration in the outlet stream. In the subsequent release step, electrochemical oxidation of the adducts triggered rapid CO_2 desorption, resulting in a sharp concentration spike until the captured CO_2 was fully released.

Notably, the high CO_2 capture capacity was consistent across cycles under both N_2 (i.e., 10% CO_2 and 90% N_2) and simulated oxygen-containing flue-gas conditions (10% CO_2, 3% O_2, and 87% N_2), demonstrating the oxygen tolerance and stability of the COF-coated electrodes (Figure 4A). The energy consumption for CO_2 capture and release also remained relatively stable across environments. Under the current density of 2 mA cm^{-2}, energy requirements were 5.06 GJ/ton for capture and 1.72 GJ/ton for release in N_2, increasing only slightly to 5.85 GJ/ton and 1.63 GJ/ton, respectively, in flue gas (Figure 4B; Table 1). Coulombic efficiencies were similarly stable, with 46% for capture and 55% for release in N_2, compared to 43% and 53% in flue gas (Figure 4C). The observed inefficiencies are likely due to incomplete formation and decomposition of the CO_2 adducts under the applied scan-potential protocol.[15] Additionally, slower diffusion and local ion depletion in the inner pore regions, compared with the outermost region of the COF, likely result in partial utilization of redox-active sites. Furthermore, the use of Na_2SO_4 as an electrolyte may also contribute to this effect during repeated cycling, as partial ion accumulation within the pores can impede ion mobility in and out of the framework.[27,46] On the other hand, incorporating extended constant-potential hold steps between cycles may potentially improve the coulombic efficiency. Long-term durability was assessed by running continuous capture/release cycles in flue gas for 80 h (Figure 4E). The CO_2 capture capacity remained above 80% of its initial value throughout the test, and the CO_2 release-to-capture ratio reached 92.2%, confirming a nearly complete release of captured CO_2 under steady-state operation. Post-cycling structural analysis further confirmed the stability of DADOP-TFP composite. PXRD patterns (Figure S36) showed reproducibility after 80 h, with minor Na_2SO_4 deposition removed upon washing. SEM images (Figure S37) revealed preserved morphology with no major structural degradation. Attenuated total reflectance infrared (ATR-IR) spectroscopy (Figure S38) indicated retention of the imine linkage and quinone framework after extended cycling.

To further elucidate the role of quinone groups in the EMCC process, we synthesized a quinone-free analog of DADOP-TFP, denoted as DADOP-QF-TFP. This controlled material was prepared as described previously, using 2,7-diaminophenanthrene (a fully reduced analog of DADOP-TFP lacking the redox-active carbonyl groups) in place of the quinone-containing amine linker. Importantly, DADOP-QF-TFP is isostructural to DADOP-TFP without the quinone sites, exhibiting the same 2D honeycomb topology, comparable pore size, and high crystallinity, as confirmed by PXRD and nitrogen sorption measurements (Figure S19). Because this material lacks the redox-active quinone units, we hypothesized that it would not exhibit CO_2 capture under analogous MEA device operation conditions. To test this hypothesis, DADOP-QF-TFP was processed into electrodes using the same ink formulation and spray-coating method described above for DADOP-TFP, and the electrodes were integrated into the MEA device under identical assembly and electrolyte conditions. When the cell potential was swept between −1.5 V and +0.5 V, no variation in CO_2 concentration was observed at the outlet of the working electrode (Figure 4D). This result confirms that the quinone units are essential for EMCC activity in this system, serving as the redox-active sites responsible for CO_2 capture and release. Furthermore, this result demonstrates that the imine linkages, while crucial for framework stability, are not themselves active toward CO_2 under these electrochemical conditions. Combined, these results confirm that electrochemical CO_2 capture in DADOP-TFP proceeds via reversible redox activity of the quinone units and occurs independently of oxygen, with no interference from competing O_2 reduction processes under operating conditions. While our results demonstrate high oxygen tolerance under simulated flue-gas conditions, it is essential to note that the gas streams employed here were limited to $O_2/CO_2/N_2$ mixtures and did not include acidic impurities such as NO_x and SO_x, which are present in real point-source flue gases and known to react with redox-active organics or promote acid-catalyzed degradation.[21,47,48] Overcoming these effects will be essential for long-term stability under realistic flue-gas environments and will be the focus of future studies.

Electronic-structure analysis using density functional theory

To further support the density functional theory (DFT)-predicted CO_2 binding pathway, we experimentally evaluated the electrochemical behavior of DAAQ and DADOP monomers under argon and CO_2 atmospheres (Figure S39). Although the monomers

Please cite this article in press as: Shehab et al., Electrified CO_2 uptake in quinone-based covalent organic frameworks, Chem (2025), https://doi.org/10.1016/j.chempr.2025.102910

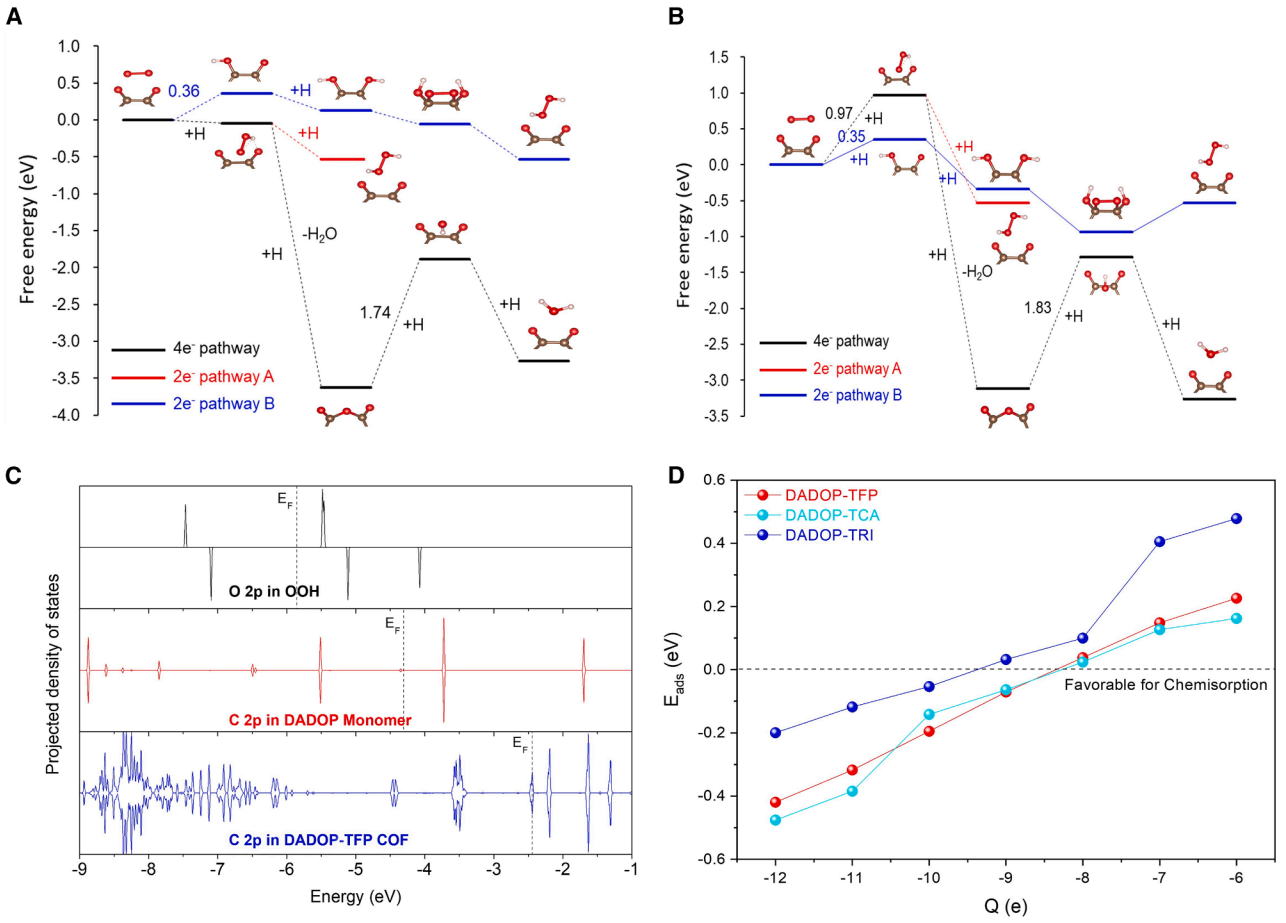

Figure 5. Free energy profiles of the 2e⁻ and 4e⁻ O_2 reduction pathways

(A and B) (A) DADOP monomer and (B) DADOP-TFP at pH = 7.

(C) PDOS of O atom in ·OOH (black), C atom in DADOP monomer (red), and C atom in DADOP-TFP (blue) (the vacuum energy level was set as the reference).

(D) Adsorption energy of CO_2 as a function of the number of additional electrons (Q) in the bulk of DADOP-TFP, DADOP-TCA, and DADOP-TRI.

show clear CO_2-dependent shifts because they are fully soluble and undergo distinct multi-step redox processes in a non-aqueous electrolyte, the COFs display nearly identical CVs under N_2 and CO_2 (Figure S40). In the solid framework, the quinone units are fixed within a rigid π-conjugated lattice and undergo a proton-coupled electron transfer (PCET)-dominated redox process in aqueous electrolyte, which smooths out the effects of CO_2. Since all DADOP-based COFs share the same redox-active unit and the linkers only weakly influence their electron density, their CV profiles naturally converge. Distinct shifts in reduction potentials and changes in wave profiles were observed upon introduction of CO_2, indicating the formation of a CO_2-quinone adduct during electrochemical reduction. These features are consistent with previously reported mechanisms for CO_2 capture by reduced quinones, as extensively demonstrated by Hatton and co-workers.[17,22]

To study and understand the electronic basis of this O_2 reduction resistance, DFT calculations were performed on both DADOP-TFP and its monomeric amine. We investigated three possible O_2 reduction pathways, including the widely studied two-electron (2e⁻) pathway A (O_2 → *OOH → H_2O_2, represented by the red lines) and the four-electron (4e⁻) pathway (O_2 → *OOH → *O + H_2O → *OH → H_2O, represented by the black lines).[49] Additionally, inspired by a previous study,[50] we examined an alternative two-electron pathway (2e⁻ pathway B), in which the oxygen atoms of the quinone C=O groups separately bind with two hydrogen atoms before forming H_2O_2 via recombination of the hydroxyl intermediates (represented by the blue lines). The DFT results reveal that the protonation of the C=O oxygen in the DADOP monomer along the 2e⁻ pathway B exhibits an energy uphill of 0.36 eV (Figure 5A). In comparison, O_2 activation to form *OOH is barrierless along both the 4e⁻ pathway and 2e⁻ pathway A, indicating these pathways are more thermodynamically favorable than 2e⁻ pathway B. Subsequently, the formation of *O + H_2O in the 4e⁻ pathway and H_2O_2 in the 2e⁻ pathway A are both exothermic, supporting their thermodynamic feasibility. The preference of the 2e⁻ pathway A explains the experimentally observed H_2O_2 production. In addition, the *O intermediate in the 4e⁻ pathway preferentially inserts between two carbon atoms, forming a C–O–C structure that may induce structural

instability and degradation of the DADOP monomer in the presence of O_2, consistent with experimental findings. In contrast, as shown in Figure 5B, although the energy uphill for protonation along $2e^-$ pathway B remains nearly unchanged (0.35 eV), the energy barriers for O_2 activation via the $4e^-$ pathway and $2e^-$ pathway A significantly increase to 0.97 eV, suggesting that DADOP-TFP exhibits reduced reactivity toward O_2 compared with its monomer. These high activation barriers help stabilize the quinone structure in the DADOP-TFP framework and thereby maintain high CO_2 capture selectivity. From Figures 5A and 5B, the higher O_2 reduction activity of the DADOP monomer is attributed to the lower energy of the *OOH intermediate, indicating stronger binding than on DADOP-TFP. To elucidate this observation, we examined the projected density of states (PDOS) of the O atom in free-standing ·OOH and the C atoms in DADOP monomer and DADOP-TFP. As shown in Figure 5C, the Fermi level (E_f) of ·OOH aligns more closely with that of the DADOP monomer compared with DADOP-TFP, resulting in stronger electronic coupling and enhanced interaction. This facilitates electron transfer (0.308 e^- from DADOP monomer to ·OOH, compared to 0.092 e^- from DADOP-TFP), thereby stabilizing the adsorbed ·OOH intermediate.

To investigate the CO_2 binding affinity of DADOP-TFP, we first examined the relationship between the partial charge of the oxygen in the C=O site (q_O) and CO_2 chemisorption energy using DFT calculations (see supplemental information, Section S4; Figures S41–S46 for details). The results reveal that across the examined charge range, DADOP-TFP consistently exhibits stronger CO_2 adsorption than the DADOP monomer (Figure S44). To gain deeper insight into the underlying electronic-structure effects, we analyzed the PDOS for CO_2 chemisorbed configurations when the partial charge of the oxygen in the C=O site (q_O) approaches approximately −0.6 e for both DADOP monomer and DADOP-TFP (Figure S45). The PDOS analysis shows that upon CO_2 adsorption, strong orbital hybridization occurs between the O 2p orbitals of the C=O site and the C 2p orbitals of CO_2, particularly in bonding σ orbitals. The introduction of additional electrons raises the Fermi level, populating more bonding states and thereby enhancing CO_2 adsorption. A comparative analysis of CO_2 at the DADOP monomer (Figure S45A) and CO_2 at DADOP-TFP (Figure S45B) reveals that the hybridized C 2p–O 2p states are more densely populated in DADOP-TFP, leading to stronger orbital overlap and interaction strength. Consequently, the electron transfer from the DADOP monomer to CO_2 is 0.54 e^-, whereas, in DADOP-TFP, it increases to 0.68 e^-, further explaining its superior CO_2 capture capability. Additionally, we compared the CO_2 adsorption energies of DADOP, DADOP-TCA, and DADOP-TRI and found that DADOP-TFP and DADOP-TCA exhibit similar performance, both outperforming DADOP-TRI. This trend aligns well with experimental observations (Figure 5D).

Conclusion

In this study, we demonstrated that integrating redox-active quinones into highly crystalline, porous COFs enables efficient and reversible electrochemical CO_2 capture by overcoming the solubility and redox-potential limitations inherent to small-molecule systems. Unlike liquid-phase electrochemical systems that require applying potential across the entire solution volume to reduce dissolved quinones, solid-state COFs localize redox activity at the sorbent interface, minimizing charge input and improving energy efficiency. A key challenge in realizing this approach was developing a scalable synthesis route to produce the gram-scale quantities of high-quality COFs required for device-level testing. To address this, we developed an open-flask method that avoids sealed ampules and enables the production of quinone-based COFs with high crystallinity and porosity at practical multi-gram scales. This approach leverages the addition of water as an additive to promote reversible imine bond formation, which facilitates error correction and the growth of high-quality COF crystals under ambient pressure. Furthermore, we established that this method is generalizable across five imine-linked COFs. Computational analysis revealed that the quinone-based COF, DADOP-TFP, exhibits a significantly narrower HOCO-LUCO gap than the quinone-based monomer, indicating enhanced electronic delocalization that contributes to improved charge transport and a positive shift in redox potential away from the region where reduction from O_2 to O_2^- occurs. To validate these results, we coated electrodes with DADOP-TFP and employed them in an MEA device under simulated flue-gas conditions (10% CO_2, 3% O_2, and 87% N_2), demonstrating high CO_2 capture capacity, stable cycling, and low-energy consumption (7.5 GJ/ton CO_2) over 80 h of continuous operation. Mechanistic studies confirmed that the quinone units serve as the active sites for capture and that the COF operates outside the O_2 reduction region, confirming operational stability in the presence of oxygen under these conditions. Complementary DFT calculations revealed that the extended COF structure hinders O_2 activation and strengthens CO_2 binding via enhanced delocalization and charge transfer. Together, our scalable synthesis strategy and device-level validation open a new avenue for CO_2 capture technology, leveraging the modularity, stability, and redox tunability of COFs for energy-efficient, electrochemically driven CO_2 separation.

METHODS

Materials

All chemicals used were purchased from commercial suppliers and utilized as received. 2,6-diaminoanthracene-9,10-dione (Ambeed, 95%); benzene-1,3,5-tricarbaldehyde (Ambeed, 96%); 4,4′,4′′-(1,3,5-triazine-2,4,6-triyl)tribenzaldehyde (Ambeed, 97%); 2,4,6-trihydroxybenzene-1,3,5-tricarbaldehyde (Ambeed, 95%); o-Iodobenzaldehyde (ChemScene, 98%); copper powder (Sigma Aldrich, 99.9%); anhydrous hydrazine (Sigma Aldrich, 98%); anhydrous tin(II) chloride (Fisher Scientific); phenanthrene-9,10-dione (Ambeed); potassium carbonate (Fisher Scientific); acetic acid (Fisher Scientific); N-Methyl-2-pyrrolidone (Sigma Aldrich, >99%); sodium sulfate (Sigma Aldrich, ACS reagent, ≥99.0%, anhydrous, powder); sodium phosphate dibasic (Sigma Aldrich ACS reagent, ≥99.0%); methanol (Fisher Scientific, 99.8%); Freudenberg H23C3, H23, and carbon black (Vulcan XC72) were purchased from Fuel Cell Store. Nafion 212 was purchased from Ion Power. Gaseous carbon dioxide (research grade), nitrogen (ultrahigh purity), and argon (ultrahigh purity) were purchased from Airgas. Ultrapure

water (18.2 MΩ from MilliQ) was used to prepare all the solutions and electrolytes.

Synthesis of building blocks and COFs

The building blocks were synthesized based on the literature with modifications (Figures 1C and S1–S12).[43,51–53] In addition, the COFs were synthesized using a generalized scaled-up procedure and characterized using PXRD, BETSI, pore size distribution (PSD), solid-state NMR, and ATR-IR measurements (Figures S13–S28). Furthermore, Pawley refinement was conducted for the AA stacking (eclipsed) model for all COFs, and the refinement parameters (R_p and R_{wp}) were calculated and tabulated (Tables S1–S5).

Scale-up synthesis of DADOP-TFP

A 250 mL 3-neck flask was charged with 100 mL NMP, DADOP (1,375 mg, 1.5 eq. amine), 2,4,6-trihydroxybenzene-1,3,5-tricarbaldehyde (TFP) (810 mg, 1.0 equiv), and 7.0 mL 6M CH_3COOH. The reaction was allowed to stir for 2 h at room temperature before 4.0 mL of water was added. The reaction was stirred overnight at room temperature at 300 rpm. The next day, the stirring was turned off, and the temperature was increased to 60°C for 15 h and then to 140°C for 4 days. The COF was washed with NMP and DMF until the filtrate became clear, then with methanol, and finally soaked in ethanol overnight for supercritical CO_2 activation to afford 2.0 g of DADOP-TFP exhibiting high crystallinity and porosity (Figures 1E and 2).

Electrode fabrication

Homogeneous ink was prepared by dispersing 150 mg COFs and 75 mg conductive carbon in 15 mL isopropanol under ultrasonication for 20 min. Subsequently, 500 mg of Nafion was added to the mixture, followed by an additional 20 min of ultrasonication to ensure uniform dispersion. The resulting ink was then spray-coated onto H23 and H23C3 carbon cloth substrates (5 cm^2 each). The coated electrode was dried at 100°C for 2 h to remove residual solvent and achieve a stable, uniform film. Composite loadings were measured at roughly 10 mg composite/cm^2 on the electrode.

Electrode hydrophilic treatment

The hydrophobic composite electrode was treated by soaking the electrodes in a 1:1 (v/v) methanol-water solution for 20 min. This process ensures thorough solvent infiltration, effectively displacing trapped air within the electrodes. Immediately after soaking, the electrodes were promptly used for MEA device assembly to maintain their wet state (Figure 1D).

Further details regarding the experimental procedures can be found in the supplemental methods.

RESOURCE AVAILABILITY

Lead contact

Further information and requests for resources and reagents should be directed to the lead contact, Omar K. Farha (o-farha@northwestern.edu).

Materials availability

This study did not generate unique reagents.

Data and code availability

All data supporting the findings of this study are included within the article and its supplemental information and are also available from the authors upon request.

ACKNOWLEDGMENTS

The authors gratefully acknowledge TotalEnergies SE for financial support. This work made use of the IMSERC crystallography facility at Northwestern University, which has received support from the Soft and Hybrid Nanotechnology Experimental (SHyNE) Resource (NSF ECCS-2025633) and the Northwestern University. This work made use of the IMSERC (RRID: SCR_017874) NMR facility at Northwestern University, which has received support from the SHyNE Resource (NSF ECCS-2025633), IIN, and Northwestern University. O.K.F. acknowledges support from the Paula M. Trienens Institute for Sustainability and Energy at Northwestern University. M.K.S. would like to acknowledge Dr. Jinlei Cui for assistance with solid-state ^{13}C NMR measurements.

AUTHOR CONTRIBUTIONS

M.K.S. and C.H. contributed equally to this work; conceptualization, M.K.S., Z.L., K.O.K., K.X., E.H.S., and O.K.F.; methodology, M.K.S., Z.L., K.O.K., K.X., E.H.S., and O.K.F.; investigation, M.K.S., Z.L., C.H., and X.W.; visualization, M.K.S., Z.L., C.H., and X.W.; funding acquisition, E.H.S. and O.K.F.; project administration, K.O.K. and K.X.; supervision: K.O.K., K.X., E.H.S., and O.K.F.; writing – original draft, M.K.S.; and writing – review & editing, M.K.S., Z.L., X.W., C.H., Y.L., K.O.K., K.X., E.H.S., and O.K.F.

DECLARATION OF INTERESTS

M.K.S., K.O.K., K.X., E.H.S., and O.K.F. are filing a patent based on this work.

SUPPLEMENTAL INFORMATION

Supplemental information can be found online at .https://doi.org/10.1016/j.chempr.2025.102910

Received: July 22, 2025
Revised: October 25, 2025
Accepted: December 14, 2025

REFERENCES

1. Ripple, W.J., Wolf, C., Gregg, J.W., Rockström, J., Mann, M.E., Oreskes, N., Lenton, T.M., Rahmstorf, S., Newsome, T.M., Xu, C., et al. (2024). The 2024 state of the climate report: Perilous times on planet Earth. BioScience *74*, 812–824. https://doi.org/10.1093/biosci/biae087.
2. Hansen, J.E., Kharecha, P., Sato, M., Tselioudis, G., Kelly, J., Bauer, S.E., Ruedy, R., Jeong, E., Jin, Q., Rignot, E., et al. (2025). Environment: Science and Policy for Sustainable Development Global Warming Has Accelerated: Are the United Nations and the Public Well-Informed? Environ.: Sci. Policy Sustain. Dev. *67*, 6–44. https://doi.org/10.1080/00139157.2025.2434494.
3. Shen, M., Kong, F., Tong, L., Luo, Y., Yin, S., Liu, C., Zhang, P., Wang, L., Chu, P.K., and Ding, Y. (2022). Carbon capture and storage (CCS): development path based on carbon neutrality and economic policy. Carbon Neutrality *1*, 37. https://doi.org/10.1007/s43979-022-00039-z.
4. Bui, M., Adjiman, C.S., Bardow, A., Anthony, E.J., Boston, A., Brown, S., Fennell, P.S., Fuss, S., Galindo, A., Hackett, L.A., et al. (2018). Carbon capture and storage (CCS): The way forward. Energy Environ. Sci. *11*, 1062–1176. https://doi.org/10.1039/c7ee02342a.
5. Kim, C., Yoo, C.J., Oh, H.S., Min, B.K., and Lee, U. (2022). Review of carbon dioxide utilization technologies and their potential for industrial application. J. CO2 Util. *65*, 102239. https://doi.org/10.1016/j.jcou.2022.102239.

6. Gizer, S.G., Polat, O., Ram, M.K., and Sahiner, N. (2022). Recent developments in CO2 capture, utilization, related materials, and challenges. Int. J. Energy Res. *46*, 16241–16263. https://doi.org/10.1002/er.8347.

7. Dziejarski, B., Krzyżyńska, R., and Andersson, K. (2023). Current status of carbon capture, utilization, and storage technologies in the global economy: A survey of technical assessment. Fuel *342*, 127776. https://doi.org/10.1016/j.fuel.2023.127776.

8. Bose, S., SenGupta, D., Rayder, T.M., Wang, X., Kirlikovali, K.O., Sekizkardes, A.K., Islamoglu, T., and Farha, O.K. (2023). Challenges and Opportunities: Metal–Organic Frameworks for Direct Air Capture. Adv. Funct. Mater. *34*, 2307478. https://doi.org/10.1002/adfm.202307478.

9. Arab, P., Parrish, E., İslamoğlu, T., and El-Kaderi, H.M. (2015). Synthesis and evaluation of porous azo-linked polymers for carbon dioxide capture and separation. J. Mater. Chem. A *3*, 20586–20594. https://doi.org/10.1039/c5ta04308e.

10. Kim, C., Talapaneni, S.N., and Dai, L. (2023). Porous carbon materials for CO2 capture, storage and electrochemical conversion. Mater. Rep. Energy *3*, 100199. https://doi.org/10.1016/j.matre.2023.100199.

11. Abdelmoaty, Y.H., Tessema, T.D., Choudhury, F.A., El-Kadri, O.M., and El-Kaderi, H.M. (2018). Nitrogen-Rich Porous Polymers for Carbon Dioxide and Iodine Sequestration for Environmental Remediation. ACS Appl. Mater. Interfaces *10*, 16049–16058. https://doi.org/10.1021/acsami.8b03772.

12. Laemont, A., Matthys, G., Lavendomme, R., and Van Der Voort, P.V. (2024). Mild and Scalable Conditions for the Solvothermal Synthesis of Imine-Linked Covalent Organic Frameworks. Angew. Chem. Int. Ed. Engl. *63*, e202412420. https://doi.org/10.1002/anie.202412420.

13. Kokoszka, B., Jarrah, N.K., Liu, C., Moore, D.T., and Landskron, K. (2014). Supercapacitive swing adsorption of carbon dioxide. Angew. Chem. Int. Ed. Engl. *53*, 3698–3701. https://doi.org/10.1002/anie.201310308.

14. Liu, C., and Landskron, K. (2017). Design, construction, and testing of a supercapacitive swing adsorption module for CO2 separation. Chem. Commun. (Camb) *53*, 3661–3664. https://doi.org/10.1039/c7cc01055a.

15. Seo, H., and Hatton, T.A. (2023). Electrochemical direct air capture of CO2 using neutral red as reversible redox-active material. Nat. Commun. *14*, 313. https://doi.org/10.1038/s41467-023-35866-w.

16. Jin, S., Wu, M., Gordon, R.G., Aziz, M.J., and Kwabi, D.G. (2020). PH swing cycle for CO2capture electrochemically driven through proton-coupled electron transfer. Energy Environ. Sci. *13*, 3706–3722. https://doi.org/10.1039/d0ee01834a.

17. Liu, Y., Ye, H.Z., Diederichsen, K.M., Van Voorhis, T., and Hatton, T.A. (2020). Electrochemically mediated carbon dioxide separation with quinone chemistry in salt-concentrated aqueous media. Nat. Commun. *11*, 2278. https://doi.org/10.1038/s41467-020-16150-7.

18. Hartley, N.A., Pugh, S.M., Xu, Z., Leong, D.C.Y., Jaffe, A., and Forse, A.C. (2023). Quinone-functionalised carbons as new materials for electrochemical carbon dioxide capture. J. Mater. Chem. A *11*, 16221–16232. https://doi.org/10.1039/d3ta02213g.

19. Voskian, S., and Hatton, T.A. (2019). Faradaic electro-swing reactive adsorption for CO2 capture. Energy Environ. Sci. *12*, 3530–3547. https://doi.org/10.1039/c9ee02412c.

20. Hartley, N.A., Xu, Z., Kress, T., and Forse, A.C. (2024). Correlating the Structure of Quinone-Functionalized Carbons with Electrochemical CO2 Capture Performance. Mater. Today Energy *45*, 101689. https://doi.org/10.1016/j.mtener.2024.101689.

21. Zito, A.M., Clarke, L.E., Barlow, J.M., Bím, D., Zhang, Z., Ripley, K.M., Li, C.J., Kummeth, A., Leonard, M.E., Alexandrova, A.N., et al. (2023). Electrochemical Carbon Dioxide Capture and Concentration. Chem. Rev. *123*, 8069–8098. https://doi.org/10.1021/acs.chemrev.2c00681.

22. Simeon, F., Stern, M.C., Diederichsen, K.M., Liu, Y., Herzog, H.J., and Hatton, T.A. (2022). Electrochemical and Molecular Assessment of Quinones as CO2-Binding Redox Molecules for Carbon Capture. J. Phys. Chem. C *126*, 1389–1399. https://doi.org/10.1021/acs.jpcc.1c09415.

23. Jing, Y., Amini, K., Xi, D., Jin, S., Alfaraidi, A.M., Kerr, E.F., Gordon, R.G., and Aziz, M.J. (2024). Electrochemically Induced CO2 Capture Enabled by Aqueous Quinone Flow Chemistry. ACS Energy Lett. *9*, 3526–3535. https://doi.org/10.1021/acsenergylett.4c01235.

24. Wielend, D., Apaydin, D.H., and Sariciftci, N.S. (2018). Anthraquinone thin-film electrodes for reversible CO2 capture and release. J. Mater. Chem. A *6*, 15095–15101. https://doi.org/10.1039/c8ta04817g.

25. Diercks, C.S., and Yaghi, O.M. (2017). The atom, the molecule, and the covalent organic framework. Science *355*, eaal1585. https://doi.org/10.1126/science.aal1585.

26. Shehab, M.K., and El-Kaderi, H.M. (2024). High Sodium Ion Storage by Multifunctional Covalent Organic Frameworks for Sustainable Sodium Batteries. ACS Appl. Mater. Interfaces *16*, 14750–14758. https://doi.org/10.1021/acsami.3c17710.

27. Shehab, M.K., Weeraratne, K.S., Huang, T., Lao, K.U., and El-Kaderi, H.M. (2021). Exceptional Sodium-Ion Storage by an Aza-Covalent Organic Framework for High Energy and Power Density Sodium-Ion Batteries. ACS Appl. Mater. Interfaces *13*, 15083–15091. https://doi.org/10.1021/acsami.0c20915.

28. Haldar, S., Roy, K., Nandi, S., Chakraborty, D., Puthusseri, D., Gawli, Y., Ogale, S., and Vaidhyanathan, R. (2018). High and Reversible Lithium Ion Storage in Self-Exfoliated Triazole-Triformyl Phloroglucinol-Based Covalent Organic Nanosheets. Adv. Energy Mater. *8*, 1702170. https://doi.org/10.1002/aenm.201702170.

29. Lei, Z., Yang, Q., Xu, Y., Guo, S., Sun, W., Liu, H., Lv, L.P., Zhang, Y., and Wang, Y. (2018). Boosting lithium storage in covalent organic framework via activation of 14-electron redox chemistry. Nat. Commun. *9*, 576. https://doi.org/10.1038/s41467-018-02889-7.

30. Ashourirad, B., Arab, P., Islamoglu, T., Cychosz, K.A., Thommes, M., and El-Kaderi, H.M. (2016). A cost-effective synthesis of heteroatom-doped porous carbons as efficient CO2 sorbents. J. Mater. Chem. A *4*, 14693–14702. https://doi.org/10.1039/c6ta06251b.

31. Rabbani, M.G., Sekizkardes, A.K., El-Kadri, O.M., Kaafarani, B.R., and El-Kaderi, H.M. (2012). Pyrene-directed growth of nanoporous benzimidazole-linked nanofibers and their application to selective CO2 capture and separation. J. Mater. Chem. *22*, 25409. https://doi.org/10.1039/c2jm34922a.

32. Ding, S.Y., Gao, J., Wang, Q., Zhang, Y., Song, W.G., Su, C.Y., and Wang, W. (2011). Construction of covalent organic framework for catalysis: Pd/COF-LZU1 in Suzuki-Miyaura coupling reaction. J. Am. Chem. Soc. *133*, 19816–19822. https://doi.org/10.1021/ja206846p.

33. Khojastehnezhad, A., Bisio, A., Rafie, S.F., Jafari, M., Peng, Z., Shehab, M.K., Abu-Zahra, N., Farha, O.K., and Siaj, M. (2025). Hierarchical Design of COFs via NHC-Grafting for Selective Gold Recovery from E-Waste: Experimental and MD Analyses. J. Am. Chem. Soc. *147*, 38516–38533. https://doi.org/10.1021/jacs.5c12234.

34. Khojastehnezhad, A., Moeinpour, F., Jafari, M., Shehab, M.K., Samih El-Douhaibi, A., El-Kaderi, H.M., and Siaj, M. (2023). Postsynthetic Modification of Core–Shell Magnetic Covalent Organic Frameworks for the Selective Removal of Mercury. ACS Appl. Mater. Interfaces *15*, 28476–28490. https://doi.org/10.1021/acsami.3c02914.

35. Jiang, Y., Liu, C., and Huang, A. (2019). EDTA-Functionalized Covalent Organic Framework for the Removal of Heavy-Metal Ions. ACS Appl. Mater. Interfaces *11*, 32186–32191. https://doi.org/10.1021/acsami.9b11850.

36. Fang, Q., Wang, J., Gu, S., Kaspar, R.B., Zhuang, Z., Zheng, J., Guo, H., Qiu, S., and Yan, Y. (2015). 3D Porous Crystalline Polyimide Covalent Organic Frameworks for Drug Delivery. J. Am. Chem. Soc. *137*, 8352–8355. https://doi.org/10.1021/jacs.5b04147.

37. Meng, Z., Aykanat, A., and Mirica, K.A. (2019). Proton Conduction in 2D Aza-Fused Covalent Organic Frameworks. Chem. Mater. *31*, 819–825. https://doi.org/10.1021/acs.chemmater.8b03897.

38. Mulzer, C.R., Shen, L., Bisbey, R.P., McKone, J.R., Zhang, N., Abruña, H.D., and Dichtel, W.R. (2016). Superior charge storage and power density of a conducting polymer-modified covalent organic framework. ACS Cent. Sci. *2*, 667–673. https://doi.org/10.1021/acscentsci.6b00220.

39. Shehab, M.K., Kaid, M.M., Pokhrel, S., Farha, O.K., and El-Kaderi, H.M. (2025). Metalated Covalent Organic Frameworks as Electrocatalytic Sulfur Cathodes for High-Performance Lithium–Sulfur Batteries. ACS Appl. Energy Mater. *8*, 12651–12660. https://doi.org/10.1021/acsaem.5c01625.

40. Alzharani, A., Shehab, M.K., Rodene, D.D., Ahmed, J.U., Bakry, A.M., Kaid, M.M., and El-Kaderi, H.M. (2022). Surface Modification of Partially Reduced Graphene Oxide for Advanced Electrode Material in Rechargeable Sodium Batteries. Energy Fuels *36*, 4967–4977. https://doi.org/10.1021/acs.energyfuels.2c00193.

41. Shehab, M.K., Weeraratne, K.S., El-Kadri, O.M., Yadavalli, V.K., and El-Kaderi, H.M. (2023). Templated Synthesis of 2D Polyimide Covalent Organic Framework for Rechargeable Sodium-Ion Batteries. Macromol. Rapid Commun. *44*, e2200782. https://doi.org/10.1002/marc.202200782.

42. Khojastehnezhad, A., Rhili, K., Shehab, M.K., Gamraoui, H., Peng, Z., Samih ElDouhaibi, A., Touzani, R., Hammouti, B., El-Kaderi, H.M., and Siaj, M. (2023). Rapid, Mild, and Catalytic Synthesis of 2D and 3D COFs with Promising Supercapacitor Applications. ACS Appl. Energy Mater. *6*, 12216–12225. https://doi.org/10.1021/acsaem.3c01913.

43. Li, M., Liu, J., Li, Y., Xing, G., Yu, X., Peng, C., and Chen, L. (2021). Skeleton engineering of isostructural 2D covalent organic frameworks: Orthoquinone Redox-active sites enhanced energy storage. CCS Chem. *3*, 696–706. https://doi.org/10.31635/ccschem.020.202000257.

44. Osterrieth, J.W.M., Rampersad, J., Madden, D., Rampal, N., Skoric, L., Connolly, B., Allendorf, M.D., Stavila, V., Snider, J.L., Ameloot, R., et al. (2022). How Reproducible are Surface Areas Calculated from the BET Equation? Adv. Mater. *34*, e2201502. https://doi.org/10.1002/adma.202201502.

45. Connelly, N.G., and Geiger, W.E. (1996). Chemical redox agents for organometallic chemistry. Chem. Rev. *96*, 877–910. https://doi.org/10.1021/cr940053x.

46. Haldar, S., Schneemann, A., and Kaskel, S. (2023). Covalent Organic Frameworks as Model Materials for Fundamental and Mechanistic Understanding of Organic Battery Design Principles. J. Am. Chem. Soc. *145*, 13494–13513. https://doi.org/10.1021/jacs.3c01131.

47. Rochelle, G.T. (2009). Amine Scrubbing for CO2 Capture. Science *325*, 1652–1654. https://doi.org/10.1126/science.1176731.

48. Kumar, A., Madden, D.G., Lusi, M., Chen, K.J., Daniels, E.A., Curtin, T., Perry, J.J., and Zaworotko, M.J. (2015). Direct Air Capture of CO2 by Physisorbent Materials. Angew. Chem. Int. Ed. Engl. *54*, 14372–14377. https://doi.org/10.1002/anie.201506952.

49. Hansen, H.A., Viswanathan, V., and Nørskov, J.K. (2014). Unifying kinetic and thermodynamic analysis of 2 e- and 4 e – reduction of oxygen on metal surfaces. J. Phys. Chem. C *118*, 6706–6718. https://doi.org/10.1021/jp4100608.

50. Zhang, X., Cheng, S., Chen, C., Wen, X., Miao, J., Zhou, B., Long, M., and Zhang, L. (2024). Keto-anthraquinone covalent organic framework for H2O2 photosynthesis with oxygen and alkaline water. Nat. Commun. *15*, 2649. https://doi.org/10.1038/s41467-024-47023-y.

51. Bacon, R.G.R., and Lindsay, W.S. (1958). 276. Cyclisations with hydrazine. Part I. The preparation of phenanthrene compounds and of pyrene from aldehydes. A variation in reductions of the Wolff–Kishner type. J. Chem. Soc. *0*, 1375–1381. https://doi.org/10.1039/JR9580001375.

52. Iuliano, A., Piccioli, P., and Fabbri, D. (2004). Ring-closing olefin metathesis of 2,2′-divinylbiphenyls: A novel and general approach to phenanthrenes. Org. Lett. *6*, 3711–3714. https://doi.org/10.1021/ol048668w.

53. Bravo, V., Gil, S., Costero, A.M., Kneeteman, M.N., Llaosa, U., Mancini, P.M.E., Ochando, L.E., and Parra, M. (2012). A new phenanthrene-based bis-oxime chemosensor for Fe(III) and Cr(III) discrimination. Tetrahedron *68*, 4882–4887. https://doi.org/10.1016/j.tet.2012.03.089.